Landslides
DOI 10.1007/s10346-015-0622-1
Received: 1 April 2014
Accepted: 30 July 2015

H. Petschko · R. Bell · T. Glade

Effectiveness of visually analyzing LiDAR DTM derivatives for earth and debris slide inventory mapping for statistical susceptibility modeling

Abstract Landslide inventories are the most important data source for landslide process, susceptibility, hazard, and risk analyses. The objective of this study was to identify an effective method for mapping a landslide inventory for a large study area (19,186 km²) from Light Detection and Ranging (LiDAR) digital terrain model (DTM) derivatives. This inventory should in particular be optimized for statistical susceptibility modeling of earth and debris slides. We compared the mapping of a representative set of landslide bodies with polygons (earth and debris slides, earth flows, complex landslides, and areas with slides) and a substantially complete set of earth and debris slide main scarps with points by visual interpretation of LiDAR DTM derivatives. The effectiveness of the two mapping methods was estimated by evaluating the requirements on an inventory used for statistical susceptibility modeling and their fulfillment by our mapped inventories. The resulting landslide inventories improved the knowledge on landslide events in the study area and outlined the heterogeneity of the study area with respect to landslide susceptibility. The obtained effectiveness estimate demonstrated that none of our mapped inventories are perfect for statistical landslide susceptibility modeling. However, opposed to mapping polygons, mapping earth and debris slides with a point in the main scarp were most effective for statistical susceptibility modeling within large study areas. Therefore, earth and debris slides were mapped with points in the main scarp in entire Lower Austria. The advantages, drawbacks, and effectiveness of landslide mapping on the basis of LiDAR DTM derivatives compared to other imagery and techniques were discussed.

Keywords Visual analysis · Landslide inventory · Mapping effectiveness · LiDAR DTM · Statistical susceptibility modeling

Introduction

Landslide inventories are a very important source to better understand landslide processes, their activity, magnitude and frequency, predisposing and preparatory factors, and landslide susceptibility and also contribute to related hazard, vulnerability, and risk analysis (Soeters and Van Westen 1996; Fell et al. 2008; Ghosh et al. 2012). They are also essential for evaluating the success and predictive power of any modeling approach used to model landslide susceptibility or hazard (Chung and Fabbri 2003; Beguería 2006).

The quality of landslide inventories depends on the completeness of spatial and temporal information (Malamud et al. 2004), having detail describing the characteristics of events (e.g., trigger, caused damage, landslide type), and the positional accuracy of the mapped landslides (Soeters and Van Westen 1996; Ardizzone et al. 2002; Glade et al. 2005; Galli et al. 2008; van Westen et al. 2008; Guzzetti et al. 2012; Petschko et al. 2014b). Understanding these quality characteristics can help to determine the usability of inventories for different applications. In this context, Malamud et al. (2004) introduced the term substantially complete landslide inventory. This term is referring to an inventory which includes all available information to describe the landslide activity, triggers, and susceptibility in an area, while it is assumed that no inventory can be complete.

Among all characteristics of an inventory, positional accuracy is the most important and also the minimum requirement (Aleotti and Chowdhury 1999; Fell et al. 2008; Malamud et al. 2004). In terms of landslide susceptibility modeling, positional errors can lead to producing an inaccurate and erroneous model, having an incorrect evaluation of the model performance or both (Malamud et al. 2004; van Westen et al. 2008). Such a result could be costly when applied for landslide hazard and risk management and policy development.

Fulfilling all the quality characteristics of an inventory is a challenging task given the mapping limitations associated with the available data source (e.g., archive, aerial photograph, satellite imagery, Light Detection and Ranging (LiDAR)), the general subjectivity inherent in mapping techniques, whether in the field or digitizing landslides from digital data sources, and human activity influencing the visibility of landslides (Cardinali et al. 2000; Ardizzone et al. 2002; van Westen et al. 2008; Fiorucci et al. 2011; Bell et al. 2012). Producing a quality inventory can become even more challenging when attempting to create a small to medium scale inventory (1:25,000; Fell et al. 2008) for a large area, since the available resources for mapping landslides are usually restricted (Van Westen et al. 1997).

Landslide inventory mapping methods are constantly evolving as new technologies and equipment become available (Guzzetti et al. 2012). An overview of traditional techniques and recent developments for landslide inventory mapping is given by Van Westen et al. (2008) and Guzzetti et al. (2012). In particular, developments in improving landslide monitoring equipment and availability of digital imagery have led to more effectiveness in reconnaissance as well as desktop mapping of landslides, which has made it easier to map landslides with higher precision and accuracy for large areas (van Westen et al. 2008; Guzzetti et al. 2012). These include GPS-equipped binoculars (Santangelo et al. 2010) and high-resolution remote sensing imagery such as (stereoscopic) optical satellite imagery (e.g., Fiorucci et al. 2011; Ardizzone et al. 2013), imagery derived from airborne or terrestrial Synthetic Aperture Radar (SAR; e.g., Colesanti and Wasowski 2006; Herrera et al. 2010; Cigna et al. 2012), and airborne or terrestrial laser scanning data (e.g., Schulz 2004; Jaboyedoff et al. 2010). This new data or imagery has recently been applied for semi-automated landslide detection on the basis of high-resolution satellite imagery as presented among others by Whitworth et al. (2005), Barlow et al. (2006), Fiorucci et al. (2011), Harp et al. (2011), and Mondini et al. (2011). Also, object-oriented approaches for detecting landslides by the combined

Published online: 20 August 2015

analysis of digital terrain model (DTM) and optical satellite data were applied recently as presented among others by Martha et al. (2010, 2012) and Stumpf et al. (2013).

Perhaps, one of the most prominent recent developments has been the utilization of high-resolution digital terrain models (DTMs and topographic derivatives) from airborne laser scanning (ALS) and LiDAR data for landslide mapping (Chigira et al. 2004; Schulz 2004; Haneberg et al. 2005; Glenn et al. 2006; Bell 2007; Anders and Seijmonsbergen 2008). Not only does this approach provide the ability to utilize highly detailed topographic data to assist with the interpretation of morphological features associated with landslides, it also allows us to overcome a major limitation of mapping from aerial imagery as the morphology underneath the forest cover can be observed (Van Den Eeckhaut et al. 2007). Additionally, mapping from airborne LiDAR data has improved our ability to effectively detect and map landslides with higher precision in positional accuracy for a larger spatial coverage. However, deriving the landslides age from airborne LiDAR data is difficult (Goetz et al. 2014), which makes analyzing the triggering conditions of the mapped landslides impractical (Petschko et al. 2014a). We refer to such an inventory where all visible landslides, regardless of age, are mapped as a historical inventory (Malamud et al. 2004).

Further advances of these methods based on the usage of derivatives from DTMs of airborne laser scanning data (LiDAR data) include semi-automated detection of landslides (e.g., van Asselen and Seijmonsbergen 2006; McKenna et al. 2008; Dalyot et al. 2008; Booth et al. 2009; Tarolli et al. 2012) and an object-oriented approach for detecting landslides under forest cover (Van Den Eeckhaut et al. 2012).

While traditionally landslides in our study area Lower Austria were mapped on topographic maps (1:50,000), a new level of positioning precision and accuracy of the landslide mapping can be reached with recently available high-resolution data (orthophotos, LiDAR DTM; Petschko et al. 2010). The objective of this study is to assess and compare the effectiveness of mapping a historical landslide inventory using polygon or point features by visually analyzing airborne LiDAR DTM derivatives. We define mapping effectiveness as an estimate comparing the time per person needed for mapping a specific number of landslides (and their attributes) with the highest possible quality in a given area, with the planned usage of the resulting inventory. Since this research is closely related to a landslide susceptibility assessment presented by Petschko et al. (2014b), it focuses on producing an earth and debris slide inventory used for statistical landslide susceptibility modeling. In particular, we wanted to answer how to effectively create an inventory for modeling a 1:25,000 scale landslide susceptibility map that covers an area of more than 19,000 km^2 and that is applied in provincial and municipal land use planning strategies (Petschko et al. 2013; Petschko et al. 2014b).

Study area

Three test districts Amstetten, Baden and Waidhofen/Ybbs were selected for assessing the most effective method of inventory mapping applicable for Lower Austria. The districts are considered as representative of the lithology and topography of Lower Austria (Fig. 1). Furthermore, they are characterized by a different number of reported landslides (mainly slide processes) in the so-called building ground register, an archive run by the Geological Survey of Lower Austria (Schwenk 1992). This allowed us to test the mapping in areas of different landslide documentation density.

The lithology of the test study area includes clastic sediments of the Molasse Zone, a unit of loess and loam, sandstone interbedded with marl in the Flysch Zone, limestone (with marls) and dolostone in the Austroalpine Unit, granite and gneiss in the Bohemian Massif, and sand, gravel, and clay in the Intramontane Basin (Fig. 1; Wessely 2006). These units show a very distinct general susceptibility to landslides given by the differences in the predominant material (Petschko et al. 2010; Petschko et al. 2014b). Furthermore, the lithological map of the study area contains a unit named "landslide deposits." This unit was assigned for areas where landslides were observed abundantly, and no information on the underlying lithology is available (Wessely 2006). However, not all landslides visible in the LiDAR DTM were assigned as "landslide deposits" in the lithological map. Furthermore, drawbacks of the map scale (1:200,000) have to be considered.

The main landslide processes in Lower Austria are shallow and deep-seated earth and debris slides (as defined by Cruden and Varnes 1996) with reported depths ranging from less than 1 m to more than 6 m (Schwenk 1992). Furthermore, earth and debris flows, rock slides, and rock falls occur. However, in this study, we focus on sliding processes (earth and debris slides and complex slides) and earth flows. Most sliding processes were reported in the Flysch Zone (Schwenk 1992). Furthermore, many slides are documented in the Klippen Zone, Molasse Zone, and the Austroalpine Unit with limestone and marl (Schwenk 1992). The high number of landslides in the Flysch and Klippen Zone and in the Austroalpine Unit and the Molasse Zone is related to the occurrence of large amounts of clays and marls in these units (Schwenk 1992).

In addition to the different observed landslide density, also the characteristics of the sliding process and morphology are different between the lithological units. While in the Molasse Zone landslides already occur at a slope angle of 5–10°, in the Flysch Zone, the slope angle is much steeper (15–25°; Schweigl and Hervás 2009). The largest slides were reported in the Molasse Zone (approx. 125,000 m^2) and the Permo-Mesozoic rocks (larger than 300,000 m^2; Schwenk 1992). In general, 35 % of the reported slides were smaller than 500 m^2 and 40 % were larger than 500 m^2 and smaller than 3,000 m^2.

During the past 60 years (1953–2011), 535 landslides were reported in the building ground register for the district Amstetten (1,187 km^2), 7 landslides were documented in Baden (754 km^2), and 151 landslides were filed for Waidhofen/Ybbs (131 km^2; Petschko et al. 2013). Associated damage occurred mainly on farmland (43 %) as well as on private houses and on infrastructure (23 %) (Petschko et al. 2010; Petschko et al. 2012).

The main triggers of earth and debris slides in Lower Austria are exceptional rainfall and/or intensive snow melt events (Schwenk 1992; Schweigl and Hervás 2009). Earthquakes occur rarely (Eisinger et al. 1992) but have not been analyzed as a landslide trigger in Lower Austria so far. The distribution of the mean annual precipitation rates (between 2001 and 2010) throughout Lower Austria shows a gradient from low rates in the northeast (500 mm) to high rates in the southwest (1,600–1,700 mm, Hydrographischer Dienst des Landes

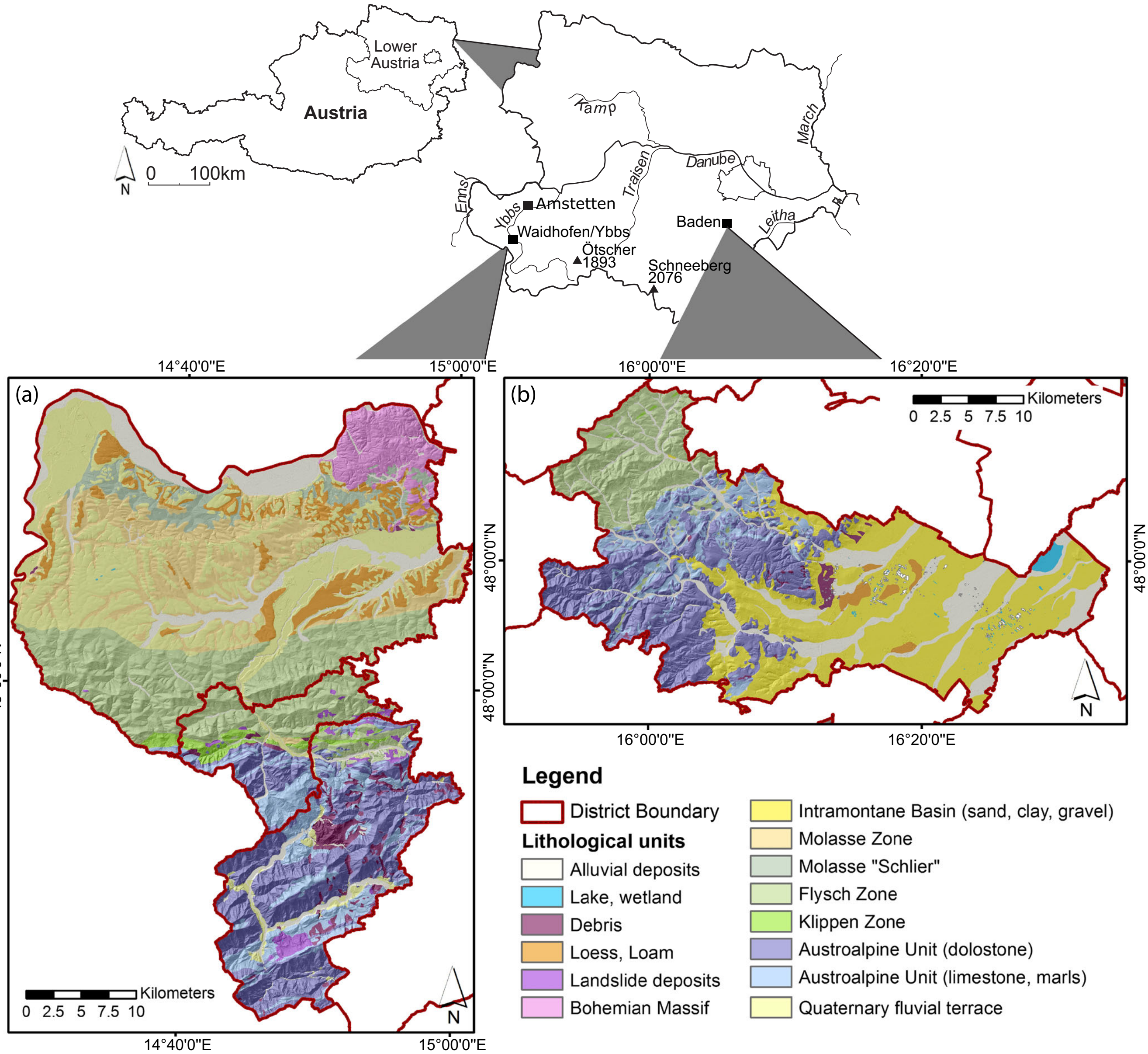

Fig. 1 Location and lithology of the three test districts **a** Amstetten, Waidhofen/Ybbs, and **b** Baden. Source: DTM: Provincial Government of Lower Austria; Lithological map: Geological Survey of Austria (GBA-2009-Zl. 383/1-09)

Niederösterreich 2011). Likewise, the station Hinterlug in the district Waidhofen/Ybbs showed a mean annual precipitation of 1,379 mm with a daily maximum of 130.5 mm measured on September 6, 2007 (Hydrographischer Dienst des Landes Niederösterreich 2011). At the station Alland in Baden, comparably low mean annual precipitation rates of 820 mm were recorded, whereas the daily maximum was very high (131.4 mm, measured on June 6, 2002; Hydrographischer Dienst des Landes Niederösterreich 2011).

Materials

The landslide inventories in this study were mapped from LiDAR DTM data that was available with a spatial resolution of 1 m×1 m. The associated airborne laser scanner flight campaigns were between 2006 and 2009 (Amt der NÖ Landesregierung 2013). Four different LiDAR platforms were used, as the flight campaigns were operated by different companies and in different years: Riegl LMS-Q560 (Riegl 2010), ALTM 3100 (Optech 2008a), ALTM Gemini (Optech 2008b), and Leica ALS50 (Leica Geosystems 2003; Amt der NÖ Landesregierung 2013).

Topographic derivatives for interpreting landslide morphology were computed in ArcGIS 9.3 from the LiDAR DTM: hillshade maps calculated with different azimuth angles (315°, 135°, 45°), a slope map displayed in inverted grayscale, and contour lines with a spacing of 4 m (Petschko et al. 2013; Fig. 2). Furthermore, orthophotos with a spatial resolution of 25 and 12.5 cm taken in the periods between 2000–2004 and 2007–2008, respectively, were available (Amt der NÖ Landesregierung 2013). Also, lithology information was derived

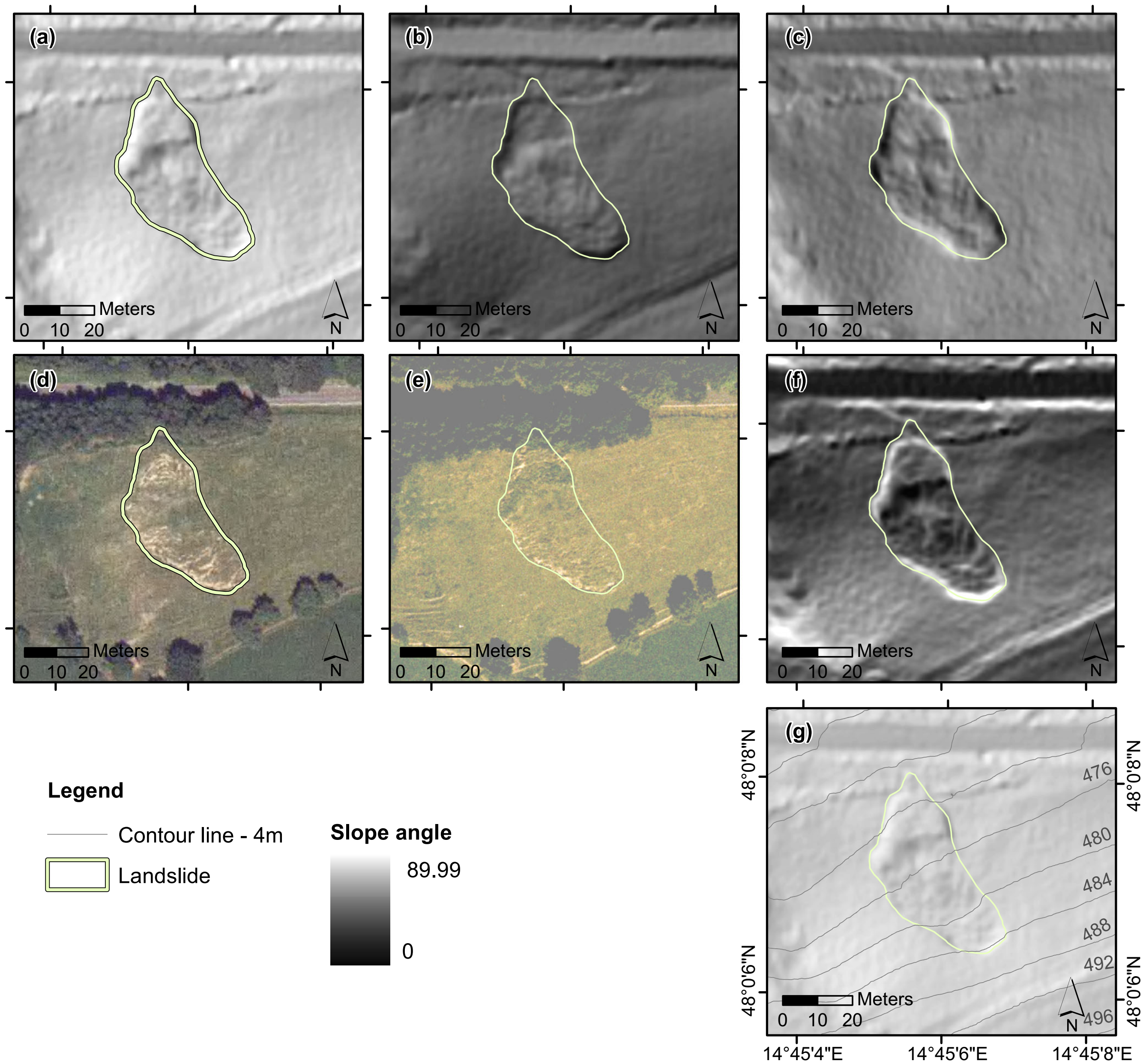

Fig. 2 A comparison of materials used for the landslide mapping: **a** Hillshade map derived from the LiDAR DTM with an azimuth angle of 315°; **b** Hillshade map derived with an azimuth angle of 135°; **c** Hillshade map derived with an azimuth angle of 45°; **d** Orthophoto (25 cm×25 cm) acquired between 2000 and 2004; **e** Orthophoto (12.5 cm×12.5 cm) acquired between 2007 and 2008; **f** Slope map derived from the LiDAR DTM; **g** Contour lines derived from the LiDAR DTM with 4-m spacing. Source: DTM and orthophotos: Provincial Government of Lower Austria; landslide mapping: own survey

from a geological map of Lower Austria at the scale 1:200,000 (Schnabel 2002).

To meet the challenge of mapping landslide bodies with polygons in a large area with restricted resources, we further developed and tested a mapping strategy in the three test districts as previously presented in Petschko et al. (2010, 2013). In these studies, our goal was to map a representative subset of landslide bodies with polygons in all lithological units using LiDAR DTM derivatives. We did not map all visible landslides but ascertained to map a representative number of landslides of all sizes and types in each lithological unit. The resulting landslide inventory stored polygons delineating landslide bodies and was available for the comparison of the effectiveness of landslide inventory mapping methods in this study. More details on the mapping methodology and the resulting inventory are given in the "Methods" and "Results" section.

Methods

We used the available LiDAR DTM and its derivatives and compared the mapping of polygons outlining the entire landslide body and the mapping of main scarps using a point per scarp regarding its effectiveness. During the mapping of landslide bodies, the landslide types of earth and debris slides, earth flows, complex sliding processes (as defined by Cruden and Varnes (1996)), and "areas with slides" were distinguished. Continuing from here, we address these different types when using the more general word landslide. However, the points were only set in scarps of earth and debris slides as it was decided to focus on these processes in the susceptibility modeling.

In the following, we introduce the general mapping method, while in the subsections, we address the specific details of mapping landslides with polygons and with a point in the main earth or debris slide scarp. The mapping method in both applications was to visually interpret the remote sensing imagery (LiDAR DTM derivatives and orthophotos; Fig. 2) regarding discernible (morphological) features remaining after landslide occurrence (Carrara and Merenda 1976; McCalpin 1984; Wieczorek 1984; Schulz 2004; Guzzetti 2005). The LiDAR derivatives (hillshades, slope map, and contour lines) and orthophotos were searched visually for a set of these typical features of earth and debris slides, earth flows, and complex sliding processes. These features include a steep concave main scarp, possibly also concave minor scarps or cracks, a landslide toe characterized by a steep convex form, irregular hummocky morphology sometimes with ridges across the slide direction, and longitudinal cracks in the toe area (Rib and Liang 1978; Varnes 1984). At minimum, a transition from a concave main scarp to a convex toe must be visible to consider the form being a slide (Guzzetti 2005). This might be recognized by a distinct change of the slope angle or of a river course due to landslide deposits as discernible on the slope angle and contour maps derived from the LiDAR DTM (Cardinali et al. 2000). The hillshades of the different azimuth angles were used to avoid shades covering landslide features hindering the delineation of the landslide boundary (Schulz 2004). The contour lines were specifically helpful to identify concave and convex features defining the main scarp and the landslide toe. Furthermore, the slope map was used to interpret steep areas which may also indicate scarps, ridges, or landslide toe (Ardizzone et al. 2007). Additional signs for landslide occurrence considered during the visual interpretation are abrupt vegetation changes from dense vegetation cover (forest, brushes, or grassland) to no cover (McCalpin 1984).

Another mapping criterion for both mapping approaches was the visual identification of all parts of the landslide (main scarp and toe) before outlining the polygon or setting the point. This reduces possible errors in the mapping due to misinterpretation of morphological convergent forms. Morphological convergence describes the presence of similar forms resulting from different natural but also anthropogenic processes (Antonini et al. 2002). Manmade features such as quarries or embankments built for houses or roads can have a similar appearance to landsliding features on the LiDAR DTM derivatives. This misinterpretation was avoided by checking the land cover on the orthophoto.

The mapping was improved and validated during detailed field surveys of exemplary, characteristic, representative, or difficultly identifiable landslides. Printouts of the LiDAR imagery and the orthophoto showing the mapped landslide and its location were prepared for each visited landslide. We aimed to visit at least one landslide per lithological unit of the test study area to learn about the specific landslide morphology and shapes and look of discernible features on the LiDAR DTM derivatives in the different lithological units. Namely, these included the unit of loess and loam, Quaternary fluvial terrace, Molasse Zone, Molasse and Schlier, Rheno-danubian Flysch Zone, Mélange Zone, Klippen Zone, Austroalpine Unit with dolostone, and the Austroalpine Unit with limestone, marl, and sandstone (Fig. 1). After locating the landslide in the field, the on-site visible borders of the landslide body and the main scarp were visually compared to the mapping. This was done to revise the desktop mapping regarding the identification of landslides, the delineation of landslide boundaries, the setting of the point in the main scarp, and the morphological convergence. Besides three earth flows, mainly earth and debris slides and areas with slides were visited to improve the mapping, which resulted in 50 field-surveyed landslides.

The landslide mapping should always be done at a larger scale than the susceptibility or hazard zoning maps to provide a thorough inventory (Cascini 2008). Given the aimed scale of the susceptibility map and the detail of the LiDAR DTM, hillshade maps and orthophotos were screened for landslide features on a scale of 1:2,000. However, the mapping (and digitizing) of the landslides was done at any larger scale necessary (1:200–1:2,000) to ensure a smooth and correct delineation of the landslide polygons and accurate and precise positioning of the landslide points.

Mapping landslide bodies with polygons

Although the methodology and selected results of mapping landslide bodies with polygons were presented in our previous studies (Petschko et al. 2010; Petschko et al. 2013), we decided to include the details in this publication to provide a full picture of the compared mapping methods. Each mapped landslide polygon was assigned with the following attributes: landslide type, relative landslide age, certainty of mapping, and certainty of the assigned type. The mapped landslide types grouped according to Cruden and Varnes (1996) were (shallow and rotational) earth and debris slides, earth flows, and complex. To speed up the mapping process, while still indicating landslide affected sites, we decided to draw one large landslide polygon around areas in which it was not so easy to distinguish between single landslides and classified this polygon as "area with slides" (Petschko et al. 2013). This area includes a slope with several landslides of different relative age, size, and maybe also type, which occurred very close or upon each other and which might also represent partial reactivations of an older landslide.

The attribute relative age was estimated according to the appearance of the landslide body morphology in the imagery (McCalpin 1984). This approach and its results are presented and discussed in more detail in Petschko et al. (2014a). The certainty of mapping and the assigned landslide type was expressed as "certain," where the type and landslide boundaries are clear and easy to detect. "Uncertain" was assigned to polygons where the boundaries were transitional and unclear or where the landslide type was ambiguous. Landslides assigned as "uncertain" were not included in the further analysis.

In addition, the mapping strategy included the mapping of landslides larger than 100 m^2 only, as this represents the area of a grid cell (10 m×10 m) planned to be applied in susceptibility modeling (Petschko et al. 2014b). Landslides below this size might be difficult to delineate on basis of the LiDAR derivatives.

Mapping earth and debris slide main scarps with points

The landslide main scarp is the most discernible part of a landslide and therefore comparably easier and faster to be detected on any imagery. At the main scarp, the best accuracy of the mapping can be achieved as the boundary between stable terrain and the failed mass particularly at the lateral boundaries, but also the toe of the landslide is often transitional (Malamud et al. 2004; Van Den Eeckhaut et al. 2006). Therefore, in contrast to the polygons, which mapped the entire landslide body, one point was used to map the main scarp of earth and debris slides. Also, instead of only mapping a representative sample, all easy discernible earth and debris slides with a fresh-looking morphology were mapped. This included mapping all identifiable earth and debris slides with fresh-looking morphology in "area with slides" instead of setting one point representing the area. Attributes describing the landslide type, relative age, or certainty of mapping were not assigned to the points. Only earth and debris slides with a high certainty of the mapping and of estimated old, young, and very young age were included in the inventory. Although assigning attributes to a single point is simple, this process can be very time consuming when mapping a very large set of points (Malamud et al. 2004).

The location of where the point should be inserted within the main scarp was patterned on a random sample done within GIS. A random sample of one point within the main scarp is frequently applied in susceptibility modeling (e.g., Atkinson et al. 1998). During the random sampling, one point is set at a random location within the main scarp area of each landslide. Adapting this for our mapping, we manually inserted one point per main scarp at a random location within the main scarp of the identified earth or debris slide.

Comparing landslide polygons and points

As an estimate on the success of the representative mapping of the landslide polygons, we calculated and compared the landslide density of each inventory (polygon or point) and the landslide ratio (RR_l) within the lithological units (l). The landslide density (D_l) is calculated by dividing the number of landslides mapped in the lithological unit (N_l) by the area of the unit (km², A; $D_l=N_l/A$). The landslide ratio (RR_l) was derived by dividing the percentage of earth and debris slides mapped as polygons within the lithological unit by the respective percentage of earth and debris slide points within each lithological unit. The landslide ratio gives an estimate on the success of the representative mapping of earth and debris slides as polygons, assuming the point mapping being substantially complete. Values greater than 1 ($RR_l>1$) indicate an overrepresented mapping of earth and debris slide polygons. Hence, values less than 1 ($RR_l<1$) signal an underrepresented mapping of earth and debris slide polygons within the respective lithological unit.

We assembled a record of the needed resources (person months (PM), working 40 h/week) for the mapping of both inventories. Furthermore, we counted the number of vertices used to map landslide bodies with polygons and main scarps with a point digitally. These numbers were used to calculate a ratio of how many more points have to be set to delineate a polygon. Both allowed estimations on the demand for mapping the entire province, given the landslide mapping rate (number of landslides in the inventory divided by person months divided by the study area size, $N_i/PM_i/A_i$; Table 1). Additionally, for the discussion of the effectiveness of the mapping method on LiDAR DTM derivatives, the obtained inventories were compared to inventories mapped by other methods (based on aerial photographs, high-resolution satellite images, semi-automated detection) as presented by Guzzetti et al. (2012) and in Table 1.

Effectiveness estimate

Comparing the effectiveness of the mapping of landslide bodies with polygons or the main landslide scarp with a point for statistical landslide susceptibility modeling, we proposed an effectiveness estimate taking into account the requirements of the modeling on the inventory. Assessing the effectiveness of the mapping of a given inventory (i) considering the type of analysis (a), we defined a semi-quantitative mapping effectiveness estimate (Ee).

Our proposed effectiveness estimate

$$\mathrm{Ee}_{ia} = \frac{N_i/\mathrm{PM}_i/A_i}{M} \times w_{ia} \tag{1}$$

takes into account the ratio of the number of landslides mapped (N) in the study area, the used resources given by the PM (working 40 h/week), and the study area size (A; km²). This landslide mapping rate was divided by the maximum value (M) of this rate of all compared inventories to obtain a value ranging between 0 and 1. Furthermore, the importance of the inventory (i; mapped polygons or points) for a specific analysis or application (a) was considered assigning a weight (w_{ia}). We performed this to make the methodology applicable and comparable for different analysis types (not only landslide susceptibility modeling).

This weight is obtained by comparing the general requirements of the given type of analysis on the inventory and the characteristics of the respective earth and debris slide inventory. We identified different requirements for statistical landslide susceptibility modeling according to general practice and recommendations in literature (Table 2). These are specifically seen in the context of the analysis of earth and debris slides and are listed below (Table 2): knowing the accurate landslide extent and/or location; knowing the date of occurrence, distinction between landslide zones (scarp, transportation, and accumulation zone), and information on the landslide runout length and/or angle of reach, landslide type, and landslide volume; and knowing the location of the main scarp, available multi-temporal information on the landslide extent, one feature (polygon/point) representatively, and one feature (polygon/point) substantially complete available per landslide and information on the triggering conditions (Van Westen et al. 1997; Guzzetti et al. 2006; Van Westen et al. 2006; Fell et al. 2008; van Westen et al. 2008). As these requirements are not equally important for statistical susceptibility modeling, we differentiated between four levels of requirements on the landslide inventory: "absolutely necessary (3 points)," "necessary (2 points)," "helpful (1 point)," and "not necessary (0 points)." For example, for statistical susceptibility modeling using grid cells as terrain units, the accurate landslide location is "absolutely necessary," whereas information on the landslide extent was considered as "helpful." We compared our mapped point and polygon inventory to the previously defined requirements evaluating if the inventory met the requirements and assigned up to 3 points according to the level of the essential information (Table 2). For example, the "absolutely necessary" accurate location of the landslides requirement was met by both our inventories. Therefore, both inventories scored 3 points. However, if one essential was not met, negative points

Table 1 Details on the mapping area, scale, imagery, number of investigators (P), time, person months (PM), number of landslides mapped (N), area mapping rate, area mapping and digitizing rate, and landslide mapping rate of the inventories compared for the inventories of this study with international examples published by Guzzetti et al. (2012)

ID	Study area	Size	Type	Scale		Imagery			Investigators (P)	
		(km^2)		Production	Publication	Type	Sets	Scale/resolution	Mapping	Digitizing
1	New Mexico, USA	315,194	G	1:100,000	1:500,000	AP	1 (2)	1:31,500; 1:12,000; 1:58,000	2	n.i.
2	Umbria, Italy	8,456	G	1:25,000	1:100,000	AP	1	1:33,000	2	1
3	Umbria, Italy	8,456	G	1:10,000	1:25,000	AP	2 (1)	1:33,000; 1:13,000; 1:73,000	4	4
4	Collazzone, Italy	79	M	1:10,000	1:10,000	AP	5	1:13,000; 1:33,000	2	1
5	Umbria, Italy	1,500	E	1:10,000	1:10,000	AP	1	1:20,000	2	n.i.
6	Imperia, Italy	500	E	1:10,000	1:10,000	AP	2 (1)	1:13,000, 1:5,000; 1:55,000	2	n.i.
7	Messina, Italy*	9.4	E	1:10,000	1:10,000	AP	2	1:3,500, 1:4,500	2.5	2
		9.4	E	1:10,000	1:10,000	SI	2	0.6 m×0.6 m	2	
8	Collazzone, Italy	10	E	1:10,000	1:10,000	LI	1	2 m×2 m	1	
9	Collazzone, Italy	79	S	1:10,000	1:10,000	SI	2	1 m×1 m, 0.5 m×0.5 m	1	
10	Test districts—polygons, Austria	2,073	G	1:2,000	1:10,000	LI	1	1 m×1 m	1	
11	Test districts—points, Austria	2,073	G	1:2,000	1:10,000	LI	1	1 m×1 m	1	
12	Lower Austria	19,186	G	1:2,000	1:25,000	LI	1	1 m×1 m	5	

ID	Time (months)		Person months (PM)	Number of landslides (N)	Area mapping rate	Area mapping and digitizing rate (km^2/P/month)	Landslide mapping rate	
	Mapping	Digitizing	Mapping + digitizing		(km^2/P/month)		(N/PM)	(N/PM/km^2)
1	18	n.i.	36	9,000	8,755	n.i.	250	0.0008
2	9	2	20	5,270	470	423	264	0.0312
3	28	20	192	47,414	100	44	247	0.0292
4	5	1	11	2,564	8	7	233	2.9505
5	6	n.i.	12	4,000	125	n.i.	333	0.2222
6	2	n.i.	4	1,204	125	n.i.	301	0.6020
7	0.58	0.16	1.8	821	6	5	463	49.2282
	0.16		0.3	821	29		2,545	270.755[a]
8	2		2	47	5		24	2.3500
9	3		3	542	26		288	0.6793

Table 1 (continued)

ID	Time (months)		Person months (PM)	Number of landslides (N)	Area mapping rate	Area mapping and digitizing rate	Landslide mapping rate	
	Mapping	Digitizing	Mapping + digitizing		(km^2/P/month)	(km^2/P/month)	(N/PM)	(N/PM/km^2)
10	4		4	1,835	518		459	0.2213
11	1.5		1.5	3,994	1,382		2,663	1.2846
12	3.2		16	13,166	1,199		823	0.0429

The original table of Guzzetti et al. (2012) was updated (marked with an asterisk (*)), partly simplified to include sliding processes mainly (where replicable from the publications), and additional information on the number of mapped landslides was added. It is distinguished between different types of inventory: geomorphological/historical inventory, event inventory, multi-temporal inventory, and seasonal inventory. Furthermore, the type of imagery is stated: aerial photograph, satellite images, and LiDAR derivatives (Guzzetti et al. 2012). The time for digitizing an inventory mapped analogue on aerial photographs was only considered where the information was available in the publications. Sources of the different data summarized in the table are listed by the ID used in the table: (1) Cardinali et al. (1990), (2) Guzzetti and Cardinali (1989), (3) Antonini et al. (2002), (4) Galli et al. (2008), (5) Cardinali et al. (2000), (6) Guzzetti et al. (2004), (7) Mondini et al. (2011), (8) Ardizzone et al. (2007), (9) Fiorucci et al. (2011), (10) Petschko et al. (2013), (11) this contribution, and (12) this contribution

G geomorphological/historical inventory, *E* event inventory, *M* multi-temporal inventory, *S* seasonal inventory, *AP* aerial photograph, *SI* satellite images, *LI* (airborne) LiDAR derivatives, *n.i.* no information was available in literature

[a] No information on single landslide polygons is available, only on areas affected by landslides

were assigned. For example, the polygon inventory did not provide the date of occurrence which is a "helpful" characteristic of the inventory for statistical modeling. Therefore, for this inventory and requirement, one negative point (−1) was assigned. Where the information could be obtained with some simple further analysis of the inventory (such as an automated derivation of main scarps from polygons delineating landslide bodies), only the half amount of points was given. As the data requirements for the analysis are also scale dependent, the mapping or analysis scale was set to range from medium (1:100,000–1:25,000) to detailed scale (>1:5,000; Fell et al. 2008).

Aiming at weights with values between 0 and 100, the sum of all points obtained by the inventory was divided by the potential amount of points and multiplied by 100. Therefore, the larger the resulting value of the effectiveness estimates the higher the effectiveness of the inventory. An effectiveness estimate below zero corresponds to a very low or no effectiveness of the given inventory for susceptibility modeling.

The inventory mapping method with the highest effectiveness for statistical landslide susceptibility modeling using grid cells as terrain unit was applied for mapping earth and debris slides in the entire province Lower Austria.

Results

Landslide body polygons and points in the main scarp

Compared to existing landslide inventories, the mapping of landslides on the LiDAR DTM derivatives revealed a large number of additional, previously unknown landslides in our test districts.

The representative mapping of landslide bodies with polygons resulted in 1,213 polygons in Amstetten, 107 polygons in Baden, and 694 polygons in Waidhofen/Ybbs (Fig. 3; Petschko et al. 2013). This totals to 2014 mapped landslide body polygons including 1,835 landslides assigned as certain of which 1,437 polygons are earth and debris slides. Among the polygons, mainly earth and debris slides (75.7 %), "areas with slides" (20.3 %), landslides classified as earth flows (3.8 %) and complex landslides (0.2 %) were mapped (Petschko et al. 2013). Nearly half of the landslide bodies mapped with polygons were considered to be of "old" relative age (48 %), whereas 34 % were assigned as "young," 10 % as "very old," and 8 % as "very young" (Petschko et al. 2014a).

Looking at the size (area in m^2) of the landslide polygons, we observed a distinct range of sizes. Seventy-five percent of the earth and debris slide bodies showed a size between 477 and 2,257 m^2 (Table 3). Besides, the size of the earth and debris slide polygons changed with the lithological unit, as shown best by the median of the boxplots (Fig. 4). The largest earth slide was mapped within the landslide deposits (1,844,305 m^2), but the smallest landslide was found in the debris, till unit (59 m^2). This shows that despite our strategy, a few landslides smaller than 100 m^2 were mapped on the LiDAR derivatives.

With the mapping of all easy discernible earth and debris slides with a "fresh" morphology with 1 point in the main scarp, even more information on earth and debris slides in the test study area was obtained. A total of 3,994 points in the main scarp were mapped in the test districts (Table 4). Two thousand seven hundred nine points in the main scarp

Table 2 Weights (w_{ia}) assigned for the importance of the polygon or point earth and debris slide inventory mapped in the test study area

Information required/given from inventory for statistical earth and debris slide susceptibility modeling	Defined requirement	Point inventory	Polygon inventory
Accurate landslide extent	1	−1	1
Accurate landslide location	3	3	3
Date of occurrence	1	−1	−1
Distinction of landslide zones (depletion, transportation, and accumulation zone)	1	0.5	0.5
Landslide runout length and/or angle of reach	1	−1	1
Landslide type distinguished	3	3	3
Location of main scarp known	3	3	1.5
One feature (point/ polygon) per landslide representative for entire study area	3	3	3
One feature (point/ polygon) per landslide substantially complete in study area	3	3	−3
Trigger or triggering conditions	1	−1	−1
Sum of (potential) points	20	11.5	8
Total weight (w_{ia}) for inventory for given application		57.5	40.0
Value "N/PM/km^2/M"[a]		1	0.2
Effectiveness estimate (Ee_{ia})[a] of inventory for given application		57.5	6.9

The information required from an inventory for statistical earth and debris slide susceptibility modeling is listed and its importance (column "defined requirement") is assigned using a point score system: "3" = absolutely necessary, "2" = necessary, and "1" = helpful (refer to Fell et al. 2008; Van Westen et al. 1997, 2008). We compared the information given by our inventory of points in the main scarp (point inventory) and our inventory of polygons marking the entire earth and debris slide body (polygon inventory) to the defined requirements (defined requirement); 0.5 up to three points were assigned respectively if the requirements were met by the inventory: absolutely necessary characteristic given → 3 points; necessary characteristic given → 2 points, helpful characteristic given → 1 point. If information could be obtained by some further analysis of the inventory, only 0.5 points were assigned. If information was required but not given by the inventory, corresponding negative points (e.g., −3 points) were allocated. The weight (w_{ia}) is the sum of the points times 100 for each inventory divided by the potential sum of score points given by the defined requirements. The resulting effectiveness estimate (Ee_{ia}; Eq. (1)) is given in the last row. The resulting value of the effectiveness estimate can range between 0 and 100, with larger values indicating a larger effectiveness of the analysed inventory mapping method regarding its usage for susceptibility modeling. The mapping or analysis scale range of the listed analysis types is from medium (1:100,000–1:25,000) to detailed scale (>1:5,000; Fell et al. 2008). Note that the values were rounded to one decimal place

[a] According to Eq. (1)

were mapped in Amstetten, 219 points in Baden, and 1,061 points in Waidhofen/Ybbs (Fig. 3).

The lithological unit with the most mapped landslides is the Rheno-danubian Flysch Zone (1,021 landslide body polygons, 2,373 points in the main scarp). However, looking at sliding processes only, the highest landslide density (D_l) was found for the Mélange Zone or also called Klippen Zone (5.09 landslide body polygons/km^2; 13.85 points in the main scarp/km^2; Table 4). The Rheno-danubian Flysch Zone ranks fourth (2.23 earth and debris slide body polygons/km^2; 6.41 points in the main scarp/km^2) following the unit of landslide deposits (4.3 earth and debris slide body polygons/km^2; 7.03 points in the main scarp/km^2) and the Molasse, Schlier unit (4.17 earth and debris slide body polygons/km^2; 8.79 points in the main scarp/km^2). Only few earth and debris slide body polygons or points in the main scarp were mapped in the alluvial deposits, Intramontane Basin and Bohemian Massif (Table 4). This comparison shows a clear difference in the landslide density of mapped earth and debris slide polygons and points in the main scarp throughout the study area which suggests a high heterogeneity in the study area regarding landslide susceptibility.

Comparing landslide polygons and points

We analyzed the success of the representative mapping of slide polygons by deriving the landslide ratio (RR_l) of the percentage of mapped earth and debris slide polygons divided by the percentage of mapped points within each lithological unit. For this ratio, we assumed that the points in the main earth and debris slide scarp represent a substantially complete sample showing all easy discernible earth and debris slides with a "fresh" morphology in the area. Generally, the results show both an underrepresented and overrepresented mapping of earth and debris slide polygons within the lithological units of the test districts (Table 4). The landslide ratio values range from 0 (in the Bohemian Massif) to a maximum of 1.7 (in the landslide deposits). Besides, earth and debris slide polygons were comparably highly overrepresented in the lithological units of debris and Intramontane Basin. Apart from the Bohemian Massif, where no earth and debris slide body polygons were mapped, the Austroalpine Unit with limestone, marl, and sandstone shows the highest underrepresentation of polygons (RR_l=0.7). Unlike this, nearly the same percentage of earth and debris slide polygons or points was found for the Rheno-danubian Flysch Zone (RR_l=0.97) and for the Mélange Zone (RR_l=1.02). In both units, the largest number of earth and debris slides was mapped.

The mapping of the polygons of all landslide types mapped as "certain" required the setting of 160,316 vertices (points) to delineate the polygons within 4 person months. The polygons of the type earth and debris slide were mapped with 100,256 vertices (points) within 1.5 person months (Table 1). Compared to the total points set in the main earth and debris slide scarp, this results in a ratio 25:1. Consequently, one could assume that the mapping of each landslide polygon needed 25 more clicks than mapping its main scarp with a point. However, it has to be kept in mind that

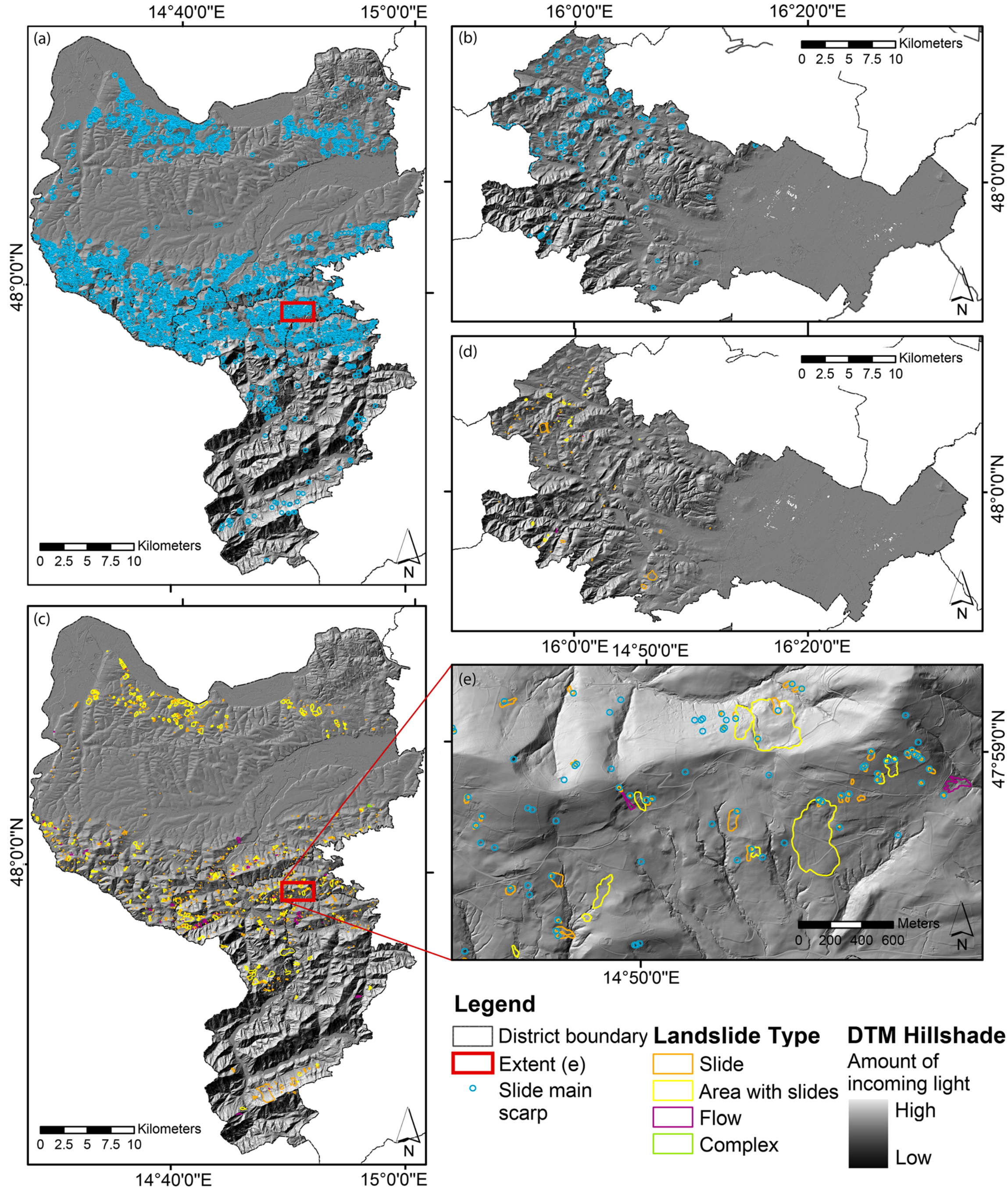

Fig. 3 Comparison of resulting landslide inventories. Landslides mapped with points (**a**, **b**) and with polygons (**c**, **d**) presented in a zoomed in example (**e**). Source: DTM: Provincial Government of Lower Austria; landslide mapping: own survey

the landslide polygons were only mapped representatively (about a third of the landslides mapped with a point). Therefore, to map one body of an earth or debris slide with a polygon, around 75 vertices have to be set opposed to one single point set in the main scarp.

The mapping of 1,834 landslide polygons took 2.67 times as many PM (working 40 h/week; 4 PM) as mapping 3,994 landslide points (1.5 PM; Table 1). This results in a landslide mapping rate of 459 and 2,663 landslides per person month, respectively (Table 1). Taking into account the size of the study area, we found that 518 km² (mapping polygons) and 1,382 km² (mapping points) were mapped per person month. Compared to studies using different mapping methods (e.g., mapping from aerial photographs or satellite images) presented by Guzzetti et al. (2012), the area mapping (and digitizing) rates were comparable but higher using LiDAR imagery in Lower Austria (Table 1). This area mapping rate was mainly dependent on the production scale of the inventory and less on the mapping method (Table 1). However, the landslide mapping rate seems to be depending on the mapping method (as shown by the imagery type used). Using aerial photographs, a

Table 3 Landslide size in square meter for the entire landslide body

Landslide type	Landslide size—body (m^2)				
	Min	1st quartile	Median	3rd quartile	Max
All types	59	595	1,408	4,203	1,844,305
Slides	59	477	971	2,257	1,844,305
Area with slides	356	4,624	10,872	36,689	746,785
Flow	274	1,616	3,283	13,400	123,566
Complex	1,546	3,229	3,740	17,724	51,935

The minimum, maximum, and median of the landslide polygon area are given. Note that the values were rounded to integers

Min minimum, *Max* maximum

lower landslide mapping rate was achieved than by mapping on satellite or LiDAR imagery (Table 1). The fastest landslide mapping rate was achieved using satellite imagery for automated detection of landslides (Table 1; Mondini et al. 2011).

Effectiveness estimate

We assessed the requirements of statistical landslide susceptibility modeling on the landslide inventory and compared these to the information given by each of the mapped inventories. We obtained a weight (w_{ia}) of 57.5 for mapping landslides with points and 40 for mapping with polygons (Table 2). Accordingly, the resulting effectiveness estimate (Ee_{ia}) was 57.5 (points) and 6.9 (polygons; Table 2).

According to our objective of statistically modeling landslide susceptibility in a large study area, visualization of the final map in three classes (Petschko et al. 2013) and the respective effectiveness estimate, the mapping of points was the preferable and acceptable method for Lower Austria. Consequently, points in the main landslide scarp were mapped for the entire province. Applying the methods to the study area Lower Austria revealed new insights into the presence of landslides in the province as 13,166 landslides were mapped in total (Fig. 5). Compared to previously existing landslide inventories, such as the building ground register of the Geological Survey of Lower Austria, we identified up to ten times more landslides in some districts.

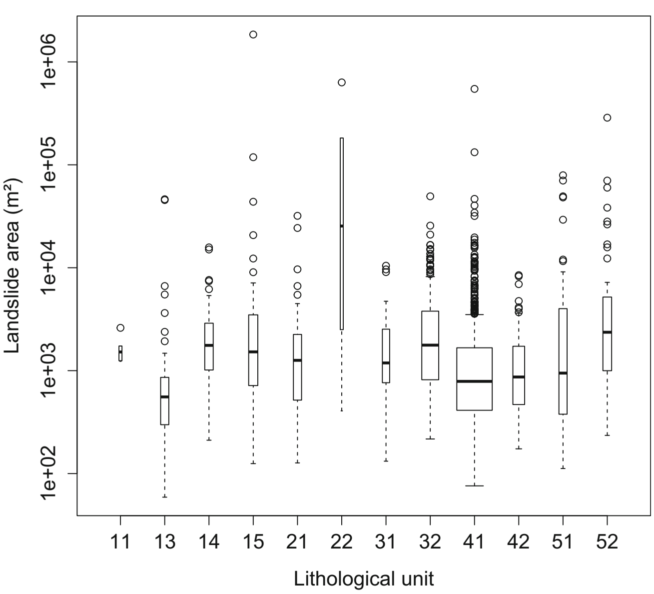

Fig. 4 Area of mapped earth and debris slide processes presented with boxplots for each lithological unit. The Bohemian Massif is not presented here, as no earth and debris slide polygons were mapped in that lithological unit. The width of the bars is relative to the number of landslides in the respective lithological unit. *Numbers* of the lithological units refer to the respective numbers given in Table 4

Discussion

Mapping landslides by visually interpreting LiDAR DTM derivatives

Generally, it is possible that the landslide features visible on the LiDAR imagery originate from recent, historical, prehistorical, or reactivated landslides. The different age or status of the landslides can be estimated from their morphology as proposed by McCalpin (1984). Depending on the age, very old or prehistoric landslides might not match the triggering conditions of today's landslides so that their inclusion in the inventory might be of disadvantage for modeling the recent landslide susceptibility. However, in our mapping approach, we focused on the mapping of easy discernible landslides with rather fresh-looking morphology only. Naturally, with this decision, it is possible that we excluded very old or possibly prehistorical slides from our mapping. However, considering easy detectable landslides accelerates the mapping process, as the decision on the delineation or the placing of a point or polygon is done faster. It reduces uncertainties introduced by erroneous delineation of the landslides without clear boundaries (Malamud et al. 2004; Van Den Eeckhaut et al. 2006).

Although we attempted to map only landslides with "easy" discernible features to ensure the quality of the inventories, the varying appearance of the landslides in the DTM derivatives across the large study area contributed to uncertainty in landslide detection. In general, it was observed that the appearance of morphological characteristics of the same landslide types (earth and debris slides) varied considerably between lithological units. This made it generally more difficult to consistently map the correct desired landslide types across the entire study area. Additionally, subdued morphological characteristics of some landslides made it generally harder to consistently map landslides accurately. Typically, these subdued characteristics are associated with older landslides (Van Den Eeckhaut et al. 2007). However, varying rates of erosion and anthropogenic modifications of landslide morphology, such as related to farming remediation activities, can also contribute to

Table 4 Comparison of the number of mapped polygons (N_{pnl}, N_{psnl}) and points (N_{ptl}), of the landslide density of mapped polygons (D_{pnl}, D_{psnl}) and points (D_{ptl}), of the landslide percentage within each lithological unit (R_{pnl}, R_{psnl}, R_{ptl}), and the landslide ratio (RR_l) in the test study area in the lithological units

ID	Lithological unit	Landslide count (N_l)			Area lith. unit (A, km^2)	Landslide density ($D_l=N_l/A$)			Landslide percentage within lithological unit ($R_l=N_l/\Sigma N_l\times 100$)			Landslide ratio ($RR_l=R_{psnl}/R_{ptl}$)
		Polygons all landslide types (N_{pnl})	Polygons "slides" (N_{psnl})	Points (N_{ptl})		Polygons (D_{pnl})	Polygons "slides" (D_{psnl})	Points (D_{ptl})	Polygons (R_{pnl}, %)	Polygons "slides" (R_{psnl}, %)	Points (R_{ptl}%)	
11	Alluvial deposits	8	6	20	231.5	0.04	0.03	0.09	0.44	0.42	0.50	0.83
13	Debris	55	44	81	33.5	1.64	1.31	2.42	3.00	3.06	2.03	1.51
14	Loess, loam	70	47	165	88.4	0.79	0.53	1.87	3.81	3.27	4.13	0.79
15	Landslide deposits	66	55	90	12.8	5.16	4.30	7.03	3.60	3.83	2.25	1.70
21	Quaternary fluvial terrace	50	44	145	275.1	0.18	0.16	0.53	2.72	3.06	3.63	0.84
22	Intramontane Basin	6	6	11	274.6	0.02	0.02	0.04	0.33	0.42	0.28	1.52
31	Molasse Zone	45	35	135	150.9	0.30	0.23	0.89	2.45	2.44	3.38	0.72
32	Molasse, Schlier	261	189	398	45.3	5.76	4.17	8.79	14.22	13.15	9.96	1.32
41	Rheno-danubian Flysch Zone	1,021	826	2,373	370.4	2.76	2.23	6.41	55.64	57.48	59.41	0.97
42	Mélange zone, Klippen Zone	127	91	248	17.9	7.10	5.09	13.85	6.92	6.33	6.21	1.02
51	Austroalpine Unit with dolostone	54	44	109	367.0	0.15	0.12	0.30	2.94	3.06	2.73	1.12
52	Austroalpine Unit with limestone, marl, and sandstone	72	50	198	149.6	0.48	0.33	1.32	3.92	3.48	4.96	0.70
61	Bohemian Massif	0	0	21	55.7	0.00	0.00	0.38	0.00	0.00	0.53	0.00
Total		1,835	1,437	3,994	2,072.7	0.89	0.69	1.93				

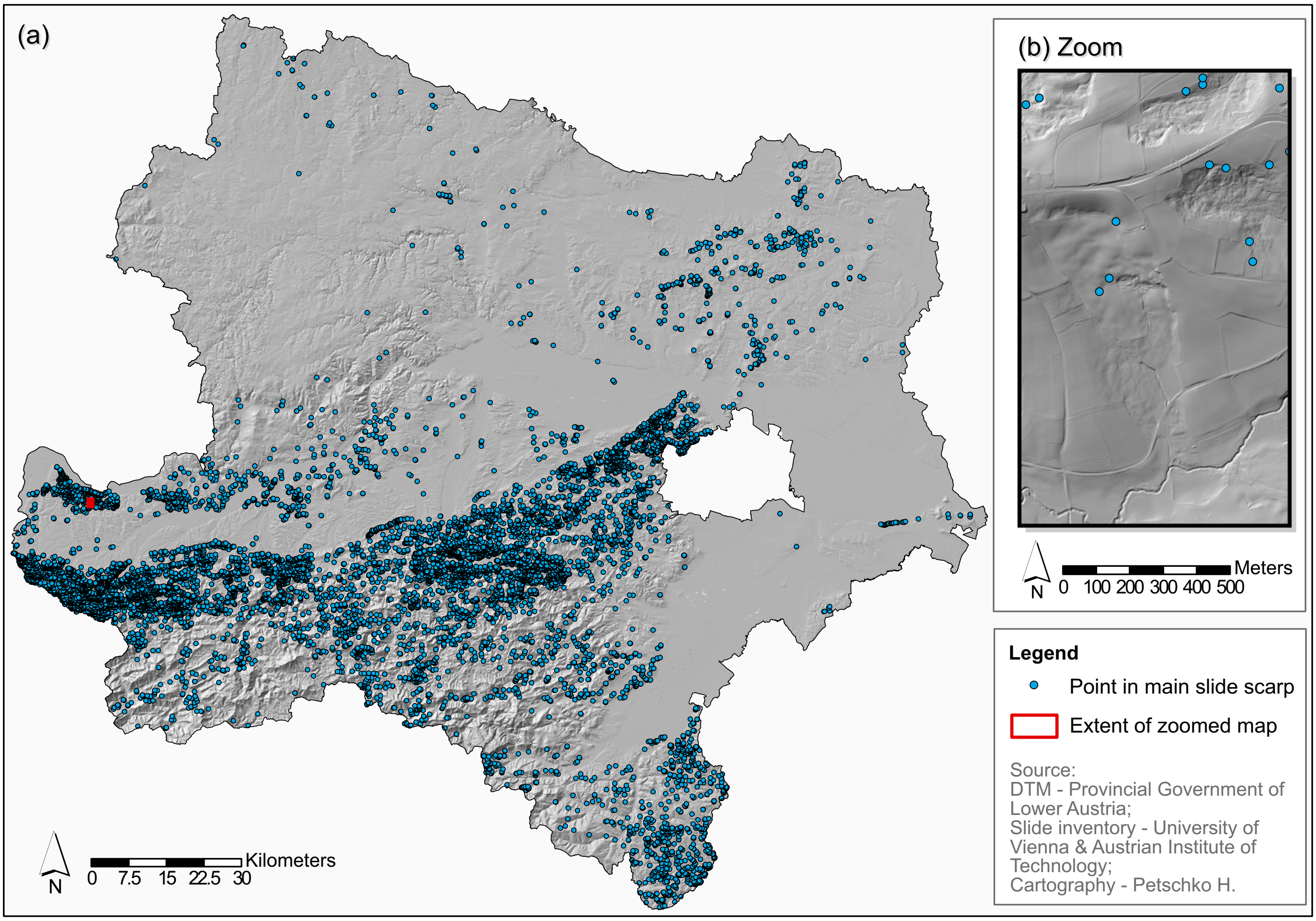

Fig. 5 **a** Resulting landslide inventory mapped using LiDAR DTM derivatives and orthophotos in Lower Austria (number of mapped main earth slide scarps=13,166). **b** Zoom to the earth and debris slides mapped in the Molasse, Schlier area in Amstetten (refer to location marked in **a** as *red dot*). Source: DTM: Provincial Government of Lower Austria; landslide mapping: own survey

the discernibility of landslides features (Fiorucci et al. 2011; Bell et al. 2012). In some cases, particularly in agricultural areas, relatively recent landslides may not be identifiable in the DTM derivatives. Accordingly, the landslide inventories may have a bias of an unknown extent towards underrepresenting landslides in agricultural land (Bell et al. 2012; Petschko et al. 2014a; Petschko et al. 2014b). Also, a conservation effect of the landslide morphological characteristics in forested areas might be present, meaning that landslide features under forest might look relatively younger than they actually are (Petschko et al. 2014a). However, a more detailed analysis is necessary to assess the presence or absence of a potential bias in our study area.

The comparison of the landslide mapping rate (N/PM) showed that semi-automated methods for landslide mapping are very fast at detecting landslides over a large area (Table 1; Mondini et al. 2011). This use of semi-automated methods for mapping landslides in large areas seems very promising, as cloud-free satellite data is usually available briefly after an event (e.g., typhoon; Martha et al. 2010; Mondini et al. 2011; Martha et al. 2012). These methods work best for large, deep-seated landslides or debris flows, where the morphological characteristics and vegetation disturbances related to the landslide are obvious. However, regarding the mapping or detection of single events, most of these advanced methods are currently lacking the possibility to delineate single landslides in highly active landslide areas. This is a disadvantage, especially when the landslide inventory should be used as a basis for statistical susceptibility modeling, when the exact location of each landslide must be known, and also when the information on how many landslides are located in a certain area is important (Petschko et al. 2014b). Therefore, an additional visual interpretation to identify the single landslides is still of high importance in landslide inventory mapping.

Mapping a representative number of landslides

The idea of mapping a representative sample only in the sense of creating a substantially complete inventory, as done in our study, might be attractive when using the resulting inventory for statistical modeling of landslide susceptibility (Calvello et al. 2013). Based on the landslides ratio (RR_l), the representative mapping of a subset of landslide bodies with a polygon was generally found to be successful. Within three lithological units out of 13, a rather high overrepresentation of mapped polygons was found (landslide deposits, debris, and Intramontane Basis). In the Rheno-danubian Flysch Zone and the Mélange Zone, the representative mapping was nearly perfect. Nevertheless, the performed expert estimation of the representativeness during the mapping might be considered as highly subjective. It seems that there is a tendency that subjectivity in mapping landslides is influenced by the landslide density. An overrepresentation of mapped landslide polygons was observed in relatively small lithological units with a high landslide density. In contrast, landslide polygons were generally observed to be underrepresented in lithological units with low landslide densities.

A more sophisticated method inspired by geospatial sampling techniques might be preferable for building a representative inventory. One such technique is the quadrat count method widely used in ecology (Krebs 1999; Christman 2000; Ver Hoef 2002; Thompson 2012). If applied to landslide mapping, this method would only map all visible landslides in a limited number of quadrats (of a specific size) randomly located in a given study area. Other approaches working with terrain mapping units of different size related to the analysis scale tested the mapping of landslides over a portion of the area for landslide susceptibility zoning (Calvello et al. 2013). In this way, full landslide information from a relatively small area can be used to calibrate and validate a model used to transfer the landslide distribution zoning maps (Calvello et al. 2013). While these spatial sampling methods sound appealing, the varying landslide conditions across our study area related to lithology, morphology, landslide size and density, and land cover pose a challenge for identifying a satisfactory and still applicable sampling technique.

Limitations of using the main scarp

The mapping (or usage) of points in the main landslide scarp leads to a limited representation of the landslide process. However, modeling with 1 point (per landslide or scarp) is a standard method used in statistical susceptibility modeling (e.g., Atkinson et al. 1998; Beguería 2006; Van Den Eeckhaut et al. 2006; Felicísimo et al. 2012). Furthermore, it is common to use the main scarp area only in the susceptibility analysis (Dai and Lee 2002; Fernández et al. 2003; Remondo et al. 2003; Santacana et al. 2003). This has consequences on the modeling results and must be considered in their further usage and interpretation. For example, many susceptibility models only estimate the spatial probability of landslide initiation, not of the run out or the entire landslide body (Petschko et al. 2014b). Assessing the entire landslide extent and the potential runout of the individual earth and debris slides is generally more important for hazard and risk analysis. A possible runout modeling solution has been proposed by Tobler et al. (2013).

Effectiveness estimate

The proposed effectiveness estimate helped to assess the requirements of statistical landslide susceptibility modeling on the inventory in a structured way. Although it might be considered as rather subjective or experimental, the resulting effectiveness estimate gave a good summary of the benefits and drawbacks of the respective inventory using it for modeling. The resulting effectiveness estimates showed that neither of the mapped landslide inventories is “perfect” for statistical landslide susceptibility modeling.

What we did not include into the effectiveness measure is the quality of the final susceptibility map (Petschko et al. 2014b). We assessed the change in the model performance and the visualization of a susceptibility map with three classes using randomly sampled points in the entire polygon or the main landslide scarp only in a logistic regression model in a previous study (Petschko et al. 2013). The resulting area under the receiver operating characteristic curve (AUROC) values were only slightly higher using points in the polygon than using points in the main scarp. Additionally, the appearance of the classified landslide susceptibility maps was similar (Petschko et al. 2013). From this modeling perspective, not only from the effectiveness estimate, we considered mapping the points in the main scarp only as an effective method as the resulting classified susceptibility maps were still reliable (Petschko et al. 2013).

Conclusions

Generally, in the best case, the landslide mapping is performed briefly after a landslide event, delineating landslide polygons and assigning as many attributes as possible. Similarly, the availability of multi-temporal data is required to analyze the potential bias of the landslide inventory towards an underrepresentation in agricultural land. However, this is a question of available resources (data, time, and trained people), the study area size and the number of landslides occurred in this area.

The restricted (multi-temporal) availability and high acquisition costs are clear limitations of the LiDAR DTM used in this study. Nevertheless, the LiDAR DTM has been proven to be of advantage for identifying and mapping landslide morphology in forested areas throughout Lower Austria for creating a historical landslide inventory.

The representative mapping of landslide polygons within the lithological units was generally found to be successful. However, the testing of more sophisticated geospatial sampling methods, such as the quadrat method taking into account the heterogeneity of the study area, is strongly recommended.

We conclude that mapping points in the main earth and debris slide scarp only is the most effective landslide inventory mapping method, in particular considering its usage in statistical landslide susceptibility modeling deriving classified susceptibility maps for large and heterogeneous study areas. However, the effectiveness estimate demonstrated that none of the mapped inventories are perfect for statistical landslide susceptibility modeling. Furthermore, the proposed effectiveness estimate might be considered as rather experimental and subjective. Despite this, it aims to help expressing the importance of an inventory for a specific analysis type. Naturally, this effectiveness estimate can be expanded or adapted for other analysis types as well.

Acknowledgments

This study was carried out within the research project “MoNOE—method development for landslide susceptibility modeling in Lower Austria” funded by the Provincial Government of Lower Austria. The authors are thankful for the provision of data by the Geological Survey of Austria and Lower Austria, the Austrian Service for Torrent and Avalanche Control, and the Provincial Government of Lower Austria. We want to thank the landslide inventory mapping team including Dr. Philip Leopold’s team at the Austrian Institute of Technology and our research assistants Mag. Christine Gassner and Ekrem Canli MSc. for their substantial work mapping landslide points in the province Lower Austria. We are grateful for the improvement of the English writing by Jason Goetz MSc. and for the thorough review and valuable comments from our anonymous reviewers, which helped in improving the quality of the manuscript.

References

Aleotti P, Chowdhury R (1999) Landslide hazard assessment: summary review and new perspectives. Bull Eng Geol Environ 58:21–44

Amt der NÖ Landesregierung (2013) Niederösterreich Atlas. http://atlas.noe.gv.at. Accessed 28 Oct 2013

Anders NS, Seijmonsbergen H (2008) Laser altimetry and terrain analysis—a revolution in geomorphology. GIM Int 36–39

Antonini G, Ardizzone F, Cardinali M, et al. (2002) Surface deposits and landslide inventory map of the area affected by the 1997 Umbria-Marche earthquakes. Boll Soc Geol It Volume speciale n.1:843–853s

Ardizzone F, Cardinali M, Carrara A et al (2002) Impact of mapping errors on the reliability of landslide hazard maps. Nat Hazards Earth Syst Sci 2:3–14

Ardizzone F, Cardinali M, Galli M, et al (2007) Identification and mapping of recent rainfall-induced landslides using elevation data collected by airborne Lidar. Nat Hazards Earth Syst Sci 7:637–650

Ardizzone F, Fiorucci F, Santangelo M, et al (2013) Very-high resolution stereoscopic satellite images for landslide mapping. In: Margottini C, Canuti P, Sassa K (eds) Landslide science and practice. Springer Berlin Heidelberg, pp 95–101

Atkinson P, Jiskoot H, Massari R, Murray T (1998) Generalized linear modelling in geomorphology. Earth Surf Process Landf 23:1185–1195

Barlow J, Franklin S, Martin Y (2006) High spatial resolution satellite imagery, DEM derivatives, and image segmentation for the detection of mass wasting processes. Photogramm Eng Remote Sens 72:687–692

Beguería S (2006) Validation and evaluation of predictive models in hazard assessment and risk management. Nat Hazards 37:315–329

Bell R (2007) Lokale und regionale Gefahren-und Risikoanalyse gravitativer Massenbewegungen an der Schwäbischen Alb. Rheinische Friedrich-Wilhelms-Universität Bonn (available at http://hss.ulb.uni-bonn.de/2007/1107/1107.htm, 29 March 2014)

Bell R, Petschko H, Röhrs M, Dix A (2012) Assessment of landslide age, landslide persistence and human impact using airborne laser scanning digital terrain models. Geogr Ann Ser Phys Geogr 94:135–156

Booth AM, Roering JJ, Perron JT (2009) Automated landslide mapping using spectral analysis and high-resolution topographic data: Puget Sound lowlands, Washington, and Portland Hills, Oregon. Geomorphology 109:132–147

Calvello M, Cascini L, Mastroianni S (2013) Landslide zoning over large areas from a sample inventory by means of scale-dependent terrain units. Geomorphology 182:33–48

Cardinali M, Guzzetti F, Brabb EE (1990) Preliminary map showing landslide deposits and related features in New Mexico. U.S. Geological Survey Open File Report 90/293, 4 sheets, scale 1:500,000

Cardinali M, Ardizzone F, Galli M, et al. (2000) Landslides triggered by rapid snow melting: the December 1996–January 1997 event in Central Italy. In: Claps P, Siccardi F (eds) Proc. 1st Plinius Conf. Bios Publisher, Cosenza, Maratea, pp 439–448

Carrara A, Merenda L (1976) Landslide inventory in northern Calabria, southern Italy. Geol Soc Amer Bull 87:1153–1162

Cascini L (2008) Applicability of landslide susceptibility and hazard zoning at different scales. Eng Geol 102:164–177

Chigira M, Duan F, Yagi H, Furuya T (2004) Using an airborne laser scanner for the identification of shallow landslides and susceptibility assessment in an area of ignimbrite overlain by permeable pyroclastics. Landslides 1:203–209

Christman MC (2000) A review of quadrat-based sampling of rare, geographically clustered populations. J Agric Biol Environ Stat 5:168–201

Chung CJ, Fabbri AG (2003) Validation of spatial prediction models for landslide hazard mapping. Nat Hazards 30:451–472

Cigna F, Bianchini S, Casagli N (2012) How to assess landslide activity and intensity with persistent scatterer interferometry (PSI): the PSI-based matrix approach. Landslides 10:267–283

Colesanti C, Wasowski J (2006) Investigating landslides with space-borne Synthetic Aperture Radar (SAR) interferometry. Eng Geol 88:173–199

Cruden DM, Varnes DJ (1996) Landslide types and processes. In: Turner AK, Schuster RL (eds) Landslides, investigation and mitigation. Transportation Research Board Special Report 247, Washington D.C., pp 36–75

Dai FC, Lee CF (2002) Landslide characteristics and slope instability modeling using GIS, Lantau Island, Hong Kong. Geomorphology 42:213–228

Dalyot S, Keinan E, Doytsher Y (2008) Landslide morphology analysis model based on LiDAR and topographic dataset comparison. Surv Land Inf Sci 68:155–170

Eisinger U, Gutdeutsch R, Hammerl C (1992) Beiträge zur Erdbebengeschichte von Niederösterreich. Amt der NÖ Landesregierung, Landesamtsdirektion, Wien, pp 154

Felicísimo ÁM, Cuartero A, Remondo J, Quirós E (2012) Mapping landslide susceptibility with logistic regression, multiple adaptive regression splines, classification and regression trees, and maximum entropy methods: a comparative study. Landslides 10:175–189

Fell R, Corominas J, Bonnard C et al (2008) Guidelines for landslide susceptibility, hazard and risk zoning for land use planning. Eng Geol 102:85–98

Fernández T, Irigaray C, El Hamdouni R, Chacón J (2003) Methodology for landslide susceptibility mapping by means of a GIS. Application to the Contraviesa area (Granada, Spain). Nat Hazards 30:297–308

Fiorucci F, Cardinali M, Carlà R et al (2011) Seasonal landslide mapping and estimation of landslide mobilization rates using aerial and satellite images. Geomorphology 129:59–70

Galli M, Ardizzone F, Cardinali M et al (2008) Comparing landslide inventory maps. Geomorphology 94:268–289

Ghosh S, van Westen CJ, Carranza EJM et al (2012) Generating event-based landslide maps in a data-scarce Himalayan environment for estimating temporal and magnitude probabilities. Eng Geol 128:49–62

Glade T, Anderson MG, Crozier MJ (2005) Landslide hazard and risk. John Wiley & Sons, Ltd, Chichester

Glenn NF, Streutker DR, Chadwick DJ et al (2006) Analysis of LiDAR-derived topographic information for characterizing and differentiating landslide morphology and activity. Geomorphology 73:131–148

Goetz JN, Bell R, Brenning A (2014) Could surface roughness be a poor proxy for landslide age? Results from the Swabian Alb, Germany. Earth Surf Process Landf 39:1697–1704

Guzzetti F, Cardinali M (1989) Carta inventario dei fenomeni franosi della Regione dell'Umbria ed aree limitrofe. CNR, Gruppo Nazionale per la Difesa dalle Catastrofi Idrogeologiche, Publication n. 204, 2 sheets, scale 1:100,000, (in Italian)

Guzzetti F (2005) Landslide hazard and risk assessment. Dissertation, Rheinischen Friedrich-Wilhelms-Universität Bonn. (Available at http://hss.ulb.uni-bonn.de/2006/0817/0817.htm, 29 March 2014)

Guzzetti F, Cardinali M, Reichenbach P, et al (2004) Landslides triggered by the 23 November 2000 rainfall event in the Imperia Province, Western Liguria, Italy. Eng Geol 73:229–245

Guzzetti F, Mondini A, Cardinali M et al (2012) Landslide inventory maps: new tools for an old problem. Earth-Sci Rev 112:42–66

Guzzetti F, Reichenbach P, Ardizzone F et al (2006) Estimating the quality of landslide susceptibility models. Geomorphology 81:166–184

Haneberg WC, Creighton AL, Medley EW, Jonas DA (2005) Use of LiDAR to assess slope hazards at the Lihir gold mine, Papua New Guinea. In: Hungr O, Fell R, Couture R, Eberhardt E (eds) Landslide risk management. Proceedings of International Conference on Landslide Risk Management. Vancouver, Canada

Harp EL, Keefer DK, Sato HP, Yagi H (2011) Landslide inventories: the essential part of seismic landslide hazard analyses. Eng Geol 122:9–21

Herrera G, Notti D, García-Davalillo JC et al (2010) Analysis with C- and X-band satellite SAR data of the Portalet landslide area. Landslides 8:195–206

Hydrographischer Dienst des Landes Niederösterreich (Hydrographic Service of Lower Austria) (2011) Wasserstandsnachrichten und Hochwasserprognosen Niederösterreich. http://www.noel.gv.at/Externeseiten/wasserstand/wiskiwebpublic/maps_N_0.htm?entryparakey=N. Accessed 2 Mar 2011

Jaboyedoff M, Oppikofer T, Abellán A et al (2010) Use of LIDAR in landslide investigations: a review. Nat Hazards 61:5–28

Krebs CJ (1999) Ecological methodology, 2nd edition. Addison-Wesley Educational Publishers Inc., Benjamin Cummings, Menlo Park, CA

Leica Geosystems (2003) ALS50 Airborne Laser Scanner, product description. Atlanta, USA, pp 10

Malamud BD, Turcotte DL, Guzzetti F, Reichenbach P (2004) Landslide inventories and their statistical properties. Earth Surf Process Landf 29:687–711

Martha TR, Kerle N, Jetten V et al (2010) Characterising spectral, spatial and morphometric properties of landslides for semi-automatic detection using object-oriented methods. Geomorphology 116:24–36

Martha TR, Kerle N, van Westen CJ et al (2012) Object-oriented analysis of multi-temporal panchromatic images for creation of historical landslide inventories. ISPRS J Photogramm Remote Sens 67:105–119

McCalpin J (1984) Preliminary age classification of landslides for inventory mapping. In: Proceedings 21st annual Engineering Geology and Soils Engineering Symposium, 5-6 April, University of Idaho, Moscow, Idaho, pp 99–111

McKenna JP, Lidke DJ, Coe JA (2008) Landslides mapped from LIDAR imagery, Kitsap County, Washington. US Geol Surv Open-File Rep 1292:81

Mondini AC, Guzzetti F, Reichenbach P et al (2011) Semi-automatic recognition and mapping of rainfall induced shallow landslides using optical satellite images. Remote Sens Environ 115:1743–1757

Optech (2008a) ALTM 3100. Optech, Canada, pp 2
Optech (2008b) ALTM Gemini. Optech, Canada, pp 2
Petschko H, Glade T, Bell R, et al. (2010) Landslide inventories for regional early warning systems. In: Malet J P, Glade T, Casagli N (eds) Proceedings of the International Conference Mountain Risks: Bringing Science to Society', Firenze, 24–26 November 2010, CERG Editions, Strasbourg, pp 277–282
Petschko H, Bell, R., Brenning A, Glade T (2012) Landslide susceptibility modeling with generalized additive models—facing the heterogeneity of large regions. In: Eberhardt E, Froese C, Turner AK, Leroueil S (eds)Taylor & Francis, Banff, Alberta, Canada, pp 769–777
Petschko H, Bell R, Leopold P, et al. (2013) Landslide inventories for reliable susceptibility maps in Lower Austria. In: Margottini C, Canuti P, Sassa K (eds) Landslide Science and Practice, Springer, pp 281–286
Petschko H, Bell R, Glade T (2014a) Relative age estimation at landslide mapping on LiDAR derivatives: revealing the applicability of land cover data in statistical susceptibility modelling. In: Sassa K, Canuti P, Yin Y (eds) Landslide science for a safer geoenvironment. Springer International Publishing, pp 337-343
Petschko H, Brenning A, Bell R et al (2014b) Assessing the quality of landslide susceptibility maps—case study Lower Austria. Nat Hazards Earth Syst Sci 14:95–118
Remondo J, González A, De Terán JRD et al (2003) Validation of landslide susceptibility maps; examples and applications from a case study in Northern Spain. Nat Hazards 30:437–449
Rib HT, Liang T (1978) Recognition and identification. In: Schuster RL, Krizek RJ (eds) Landslide analysis and control. National Academy of Sciences, Washington, pp 34–80
Riegl (2010) LMS-Q560 airborne laser scanner for full waveform analysis. Austria, Japan, USA
Santacana N, Baeza B, Corominas J et al (2003) A GIS-based multivariate statistical analysis for shallow landslide susceptibility mapping in La Pobla de Lillet area (Eastern Pyrenees, Spain). Nat Hazards 30:281–295
Santangelo M, Cardinali M, Rossi M et al (2010) Remote landslide mapping using a laser rangefinder binocular and GPS. Nat Hazards Earth Syst Sci 10:2539–2546
Schnabel W (2002) Geologische Karte von Niederösterreich 1:200,000. Geological Survey of Austria, Vienna
Schulz WH (2004) Landslides mapped using LIDAR imagery, Seattle, Washington. US Geol. Surv. Open-File Rep. 1396:11
Schweigl J, Hervás J (2009) Landslide mapping in Austria. European Commission Joint Research Centre, Institute for Environment and Sustainability, Italy, pp 65
Schwenk H (1992) Massenbewegungen in Niederösterreich 1953–1990. Jahrb. Geol. Bundesanst. Geologische Bundesanstalt, Wien, pp 597–660
Soeters R, Van Westen CJ (1996) Slope instability recognition, analysis and zonation. In: Turner AK, Schuster RL (eds) Landslides, investigation and mitigation. National Academy Press, Washington, USA, p 129-177
Stumpf A, Malet J-P, Kerle N et al (2013) Image-based mapping of surface fissures for the investigation of landslide dynamics. Geomorphology 186:12–27
Tarolli P, Sofia G, Dalla Fontana G (2012) Geomorphic features extraction from high-resolution topography: landslide crowns and bank erosion. Nat Hazards 61:65–83
Thompson SK (2012) Sampling, 3rd edn. John Wiley & Sons Inc., Hoboken, p 472
Tobler D, Riner R, Pfeifer R (2013) Runout modelling of shallow landslides over large areas with SliDepot. In: Margottini C, Canuti P, Sassa K (eds) Landslide science and practice. Springer, Heidelberg, pp 239–245
Varnes DJ (1984) Landslide hazard zonation: a review of principles and practice. United Nations Educational, Scientific and Cultural Organization, Paris, France
Van Asselen S, Seijmonsbergen AC (2006) Expert-driven semi-automated geomorphological mapping for a mountainous area using a laser DTM. Geomorphology 78:309–320. doi:10.1016/j.geomorph.2006.01.037
Van Den Eeckhaut M, Kerle N, Poesen J, Hervás J (2012) Object-oriented identification of forested landslides with derivatives of single pulse LiDAR data. Geomorphology 173–174:30–42
Van Den Eeckhaut M, Poesen J, Verstraeten G et al (2007) Use of LIDAR-derived images for mapping old landslides under forest. Earth Surf Process Landf 32:754–769
Van Den Eeckhaut M, Vanwalleghem T, Poesen J et al (2006) Prediction of landslide susceptibility using rare events logistic regression: a case-study in the Flemish Ardennes (Belgium). Geomorphology 76:392–410
Van Westen CJ, Asch TWJ, Soeters R (2006) Landslide hazard and risk zonation—why is it still so difficult? Bull Eng Geol Environ 65:167–184
Van Westen CJ, Castellanos E, Kuriakose SL (2008) Spatial data for landslide susceptibility, hazard, and vulnerability assessment: an overview. Eng Geol 102:112–131
Van Westen CJ, Rengers N, Terlien MTJ, Soeters R (1997) Prediction of the occurrence of slope instability phenomena through GIS-based hazard zonation. Geol Rundsch 86:404–414
Ver Hoef J (2002) Sampling and geostatistics for spatial data. Ecoscience 9:152–161
Wessely G (2006) Geologie der österreichischen Bundesländer-Niederösterreich. Geological Survey Austria, Vienna
Whitworth MCZ, Giles DP, Murphy W (2005) Airborne remote sensing for landslide hazard assessment: a case study on the Jurassic escarpment slopes of Worcestershire, UK. Q J Eng Geol Hydrogeol 38:285–300
Wieczorek G (1984) Preparing a detailed landslide-inventory map for hazard evaluation and reduction. G Bull Assoc Engng Geol 21:337–342

H. Petschko (✉)
Department of Geography,
Friedrich Schiller University Jena,
Löbdergraben 32, 07743, Jena, Germany
e-mail: helene.petschko@uni-jena.de

H. Petschko · R. Bell · T. Glade
Department of Geography and Regional Research,
University of Vienna,
Universitätsstrasse 7, 1010, Vienna, Austria